Direct Correlation of Carbon Nanotube Nucleation and Growth with the Atomic Structure of Re Nanocatalysts Stimulated and Imaged by the Electron Beam

Kecheng Cao,[†] *Thomas W. Chamberlain,*[‡,§] *Johannes Biskupek,*[†] *Thilo Zoberbier,*[†] *Ute Kaiser*[*,†] *and Andrei N. Khlobystov*[*,‡,∥]

[†]Electron Microscopy of Materials Science, Central Facility for Electron Microscopy, Ulm University, Albert-Einstein-Allee 11, Ulm 89081, Germany

[‡]School of Chemistry, University of Nottingham, University Park, Nottingham NG7 2RD, United Kingdom

[§] Institute of Process Research and Development, School of Chemistry, University of Leeds, Leeds LS2 9JT, United Kingdom

[∥] Nanoscale & Microscale Research Centre (nmRC), University of Nottingham, University Park, Nottingham NG7 2RD, United Kingdom

KEYWORDS: Carbon nanotube, catalysis, chemTEM, transmission electron microscopy, metal cluster

ABSTRACT: Sub-nanometre Re clusters confined in a single-walled carbon nanotube are activated by the 80 keV electron beam to promote the catalytic growth of a new carbon nanotube. Transmission electron microscopy images the entire process step-by-step, with atomic resolution in real time, revealing details of the initial nucleation followed by a two-stage growth. The atomic dynamics of the Re cluster correlate strongly with the nanotube formation process, with the growth accelerating when the catalyst becomes more ordered. In addition to the nanotube growth catalysed by Re nanoclusters, individual atoms of Re released from the nanocluster play a role in the nanotube formation.

Chemical vapor deposition (CVD) is one of the most valuable synthetic processes where inexpensive, abundant small molecules, such as methane or ethanol, are transformed, in a single step, into high-value materials, such as graphene[1] or carbon nanotubes[2]. The harsh conditions of CVD (e.g. high temperature, highly dynamic gas-solid interface) prohibit the use of traditional analytical methods and, therefore, preparative CVD has been developing mainly through empirical, trial-and-error approaches[3]. In the context of carbon nanotubes, CVD is recognized as the only viable method for mass production of these materials, but atomistic mechanisms of nanotube growth are still uncertain, for example, the state of the metal catalyst (molten or solid), the composition of the catalyst (e.g. pure metal or metal carbide), and the pathways of carbon atom transport (e.g. across the surface or through the bulk of the catalyst) are still debated. In this study, we shed light on the fundamental aspects of the nanotube formation process by establishing a

relationship between nanotube nucleation and growth, and the atomic structure of the nanocatalyst. In our experiments, transformations are promoted by energy of the electron beam, rather than heat, laser or electric arc, which allows us to follow the entire process at the atomic scale, capturing images of all key stages, allowing us to monitor directly the state of the catalyst nanocluster and simultaneously the nanotube growth, using rhenium nanoclusters as an archetypal catalyst.

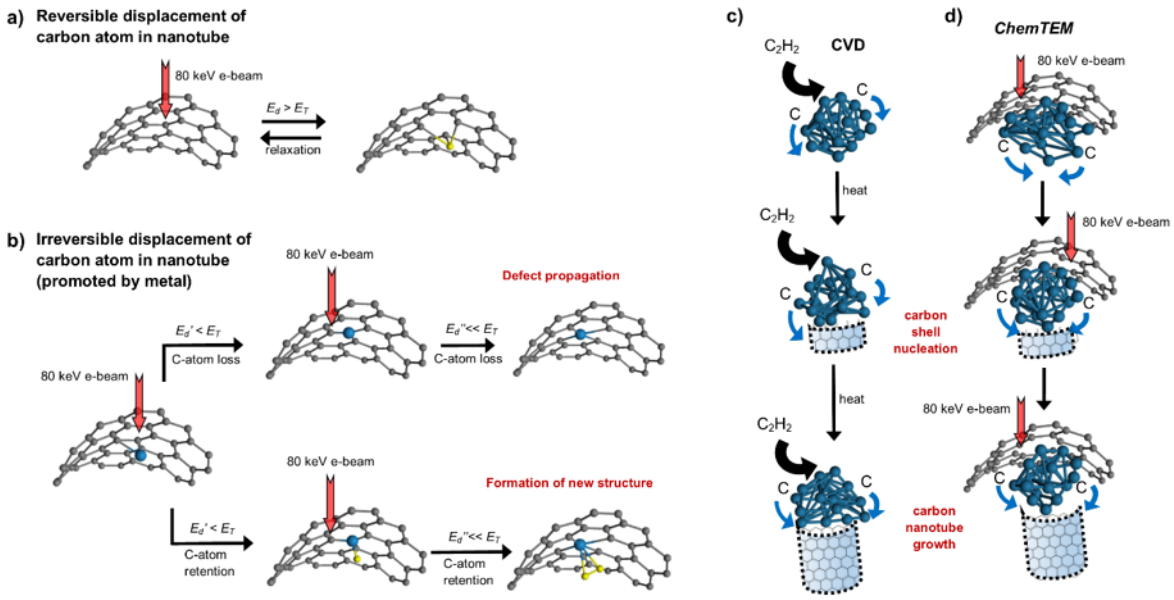

Figure 1. a) The 80 keV electron beam of TEM supplies kinetic energy to carbon atom (E_T) insufficient to overcome the barrier for irreversible displacement (E_d). However, b) in the presence of metal atom inside nanotube the barrier is lower (E_d') such that C-atoms are selectively removed from SWNT in vicinity of the metal, either leaving the system (top) or remaining adsorbed on the metal (bottom, adsorbed C-atoms are highlighted yellow). The carbon atoms displacement from SWNT and retention on metal leads to formation of new structures inside nanotube. A comparison of nanotube formation in CVD c) with *ChemTEM* (d) demonstrates that reactive carbon atoms are formed via metal catalysed decomposition of molecules or carbon nanotube sidewall respectively,

in both cases leading to diffusion of carbon atoms across the nanocatalyst to form a new nanotube structure (outlined with dotted lines).

Amongst analytical methods, environmental transmission electron microscopy (ETEM) is able to recreate the conditions of CVD synthesis and image nanotube growth at the individual nanotube level. ETEM showed, for example, that FeC_3 catalyst nanoparticles behave as fluctuating solid nanocrystals during nanotube formation, and revealed an 'incubation period' characterised by a reversible formation of metastable carbon caps, preceding a period of fast nanotube growth.[4] Similarly, another ETEM study shows a slow initial stage of carbon cap nucleation on Ni, followed by a period of fast growth.[5] Nucleation of the carbon cap (also known as the 'yarmulke' mechanism),[6] that determines the diameter, chiral indices [n,m] and functional properties of the nanotube, is recognized as a rate-limiting stage in CVD with an activation barrier of ~2.7 eV.[5] Theoretical modelling predicts that the stability of a carbon cap is dictated by a match of its atomic structure to the atomic lattice of metal catalyst during the nucleation step [7], suggesting significant epitaxial character in the nanotube formation process. In addition, Rodríguez-Manzo *et. al.* directly observed the nucleation of a nanotube on the surface of a relatively large metal nanoparticle at 600 °C in ETEM with the 300 keV e-beam being suggested to facilitate the growth of nanotube.[8]

A close relationship between the atomic structure of the catalyst surface and the nanotube structure was also proposed on the basis of highly chirality-selective nanotube growth, attributed to a well-defined atomic interface between the growing nanotube and the metal catalyst particle, for Ni_xFe_{1-x} and W_6Co_7.[9,10] However, presently there is no methodology that can probe directly the nanotube-catalyst interface, with atomic resolution, during the process of nanotube formation. While the recent developments in ETEM analysis are instructive for studying catalysis on nanoparticles, this methodology is not suitable for metal nanoclusters due to their extremely dynamic nature, and

inability to decouple the thermal effects from the contribution of the e-beam. Hence the overall atomic dynamics of nanotube nucleation and growth is not sufficiently understood to enable CVD synthesis to be rationalized.

In a CVD process, carbon is delivered to the catalyst in the form of adsorbed molecules, followed by their decomposition activated by heat or plasma. Thus, liberated reactive carbon atoms diffuse across the catalyst and join together to form a nanotube (Figure 1c). Our approach is different to ETEM as we employ a pre-formed single-walled carbon nanotube (SWNT) as a substrate for catalytic metal nanoclusters positioned within the nanotube cavity (denoted as M@SWNT). Instead of heat, we merely employ the kinetic energy of the 80 keV electron beam, a well-defined fraction of which is transferred directly to carbon atoms thus moving them from equilibrium positions, breaking bonds and generating reactive carbon atoms knocked out of the SWNT in the vicinity of the catalyst (Figure 1). The choice of the energy of the e-beam is very important, as the 80 keV e-beam transfers an amount of kinetic energy (E_T) to the individual carbon atoms that is just below the threshold required to knock a C-atom from the carbon framework of a pristine SWNT, e.g. the SWNT remains virtually intact under these conditions (Figure 1a) unless the nanotube atoms are 'activated' by direct contact with the transition metal [11,12] shown in our previous work to lower the threshold for displacement of carbon from the SWNT by the e-beam (Figure 1b).[13] Similar to CVD, the metal nanocluster in our experiments acts as a catalyst for dissociation of C-C bonds (Figure 1d), and immobilization of the catalyst inside the SWNT enables continuous, atomically-resolved imaging of its structure during chemical reactions promoted by the catalyst. Harnessing the electron beam as a promoter of chemical reactions and an imaging tool at the same time enables imaging of atomic dynamics in direct space and real time: when E_T exceeds the activation barrier for atom displacement (E_d) a reaction takes place, with the reaction

rate being controlled by the dose rate of the electron beam (j, e/nm^2·s).[14] Both, E_T and j are determined exclusively by the experimental settings of the TEM which can be readily tuned to image chemical transformations of organic or inorganic molecules – an approach named *ChemTEM*,[11,15,16] which has been successfully applied to image the atomistic mechanisms of polycondensation reactions[15,17], fullerene formation[18] and graphene nanoribbon growth[19], as well as the Stone-Wales rearrangement in graphene[20]. In this approach, the chemical nature of the metal inside the SWNT is crucially important as the metal must both be sufficiently active towards the activation of C-C bonds and be able to retain adsorbed atomic carbon generated from the SWNT by the e-beam, such that a reactive environment with a steady supply of carbon is created around the catalyst (Figure. 1b) which replicates CVD conditions. Previously, we demonstrated the unusual ability of individual Re atoms to promote rearrangement of carbon atoms in the SWNT sidewall[21], and in this study we utilize small clusters of ca. 30-60 Re atoms, embedded within SWNTs (Re@SWNT), in order to elucidate atomistic mechanisms of nanotube growth (Figure 1d).

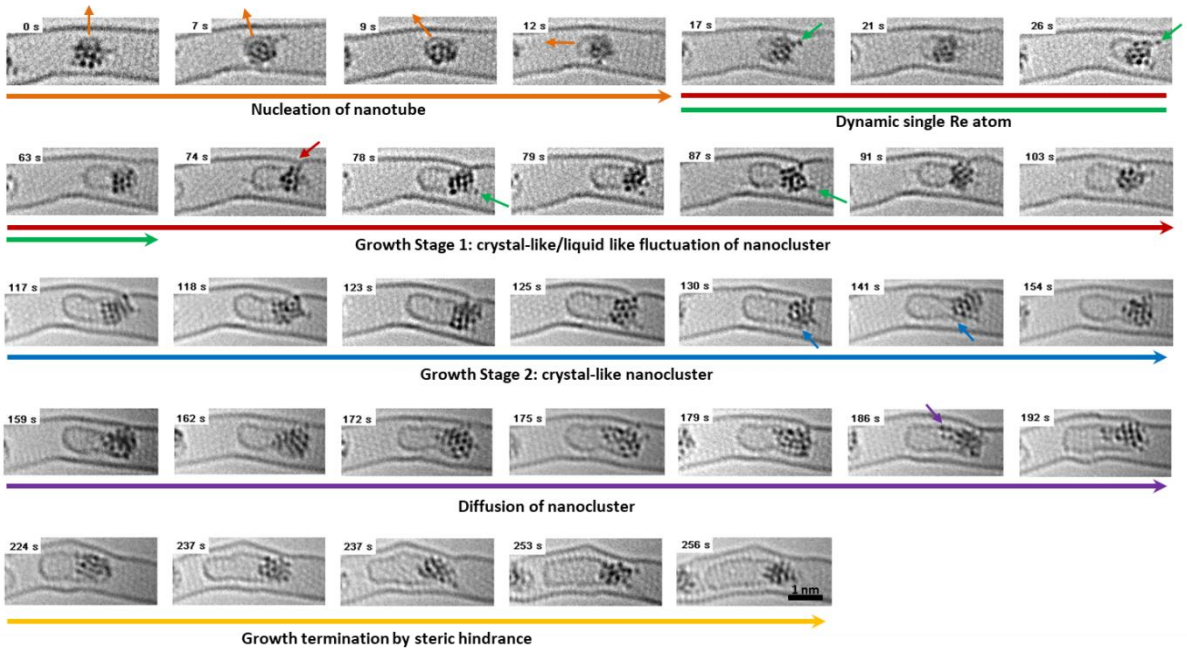

Figure 2. Time series of AC-HRTEM images following the formation of a carbon nanotube on a nanocluster of Re embedded within a host-SWNT (Re@SWNT). Orange, green, red, blue and purple short arrows indicate the direction of nanotube nucleus formation (carbon shell), positions of dynamic single Re atoms, single atom contact sites in nanotube, newly nucleated SWNT wall and diffused Re atoms respectively.

Time-series aberration-corrected high-resolution TEM (AC-HRTEM) images of Re@SWNT reveal that activated by the 80 keV e-beam at the dose rate of 1×10^6 $e^-/nm^2 \cdot s$, the Re nanocluster catalyzes the 'parasitic growth' of a new SWNT within the inner cavity of the original SWNT (Figure 2, Video S1). The identity of the metallic clusters in the nanotubes was confirmed by energy dispersive X-ray (EDX) spectroscopy using a focused 100 keV electron beam to irradiate a small bundle of 5–10 filled SWNTs (Figure 3a). The presence of Re in the SWNT clearly lowers the barrier for displacement of C-atoms (E_d') below the maximum E_T received by the carbon atoms in collisions with the 80 keV electrons and, as a result, the metal effectively promotes the formation of small defects in the SWNT sidewall. When the first one or two carbon atoms are removed from the graphenic lattice, the threshold for removal of subsequent C-atoms form the SWNT is significantly reduced by approximately 4-7 eV ($E_d'' << E_T$), such that the defect in the SWNT provides a consistent supply of atomic carbon to the metal nanocluster. Some metals, such as Os under these conditions are not able to retain atomic carbon, leading to fast defect propagation and rupture of nanotube[12], however Re nanoclusters appear to be able not only to activate the removal of C-atoms from the SWNT but also be able to adsorb an appreciable amount of C-atoms, retaining them in the SWNT cavity. A Re nanocluster confined in the middle of a SWNT (with another Re nanocluster to the right; Figure S1) and irradiated by the e-beam, catalyzes formation of a semi-

circular carbon shell after only a few seconds (Figure 2, 0 s-9 s frames). There is a clear induction period in nanotube growth (7 s–12 s) as the carbon shell capping the nanocluster grows with a slow rate of ~0.005 nm/s, whilst the shape and orientation of the carbon cap change rapidly and continuously (indicated with an orange arrow, Figure 2, frames 0 s–12 s), until an elongated shape aligned with the SWNT axis is formed (Figure 2, 12 s–17 s frames). The growth of the carbon cap is blocked in certain directions by steric hindrance from the wall of the host SWNT. Benefiting from the flexible atomic structure of the Re cluster, the carbon cap easily reorganizes its orientation on the surface of the Re cluster. During this process the carbon cap becomes the nucleus of the future nanotube.

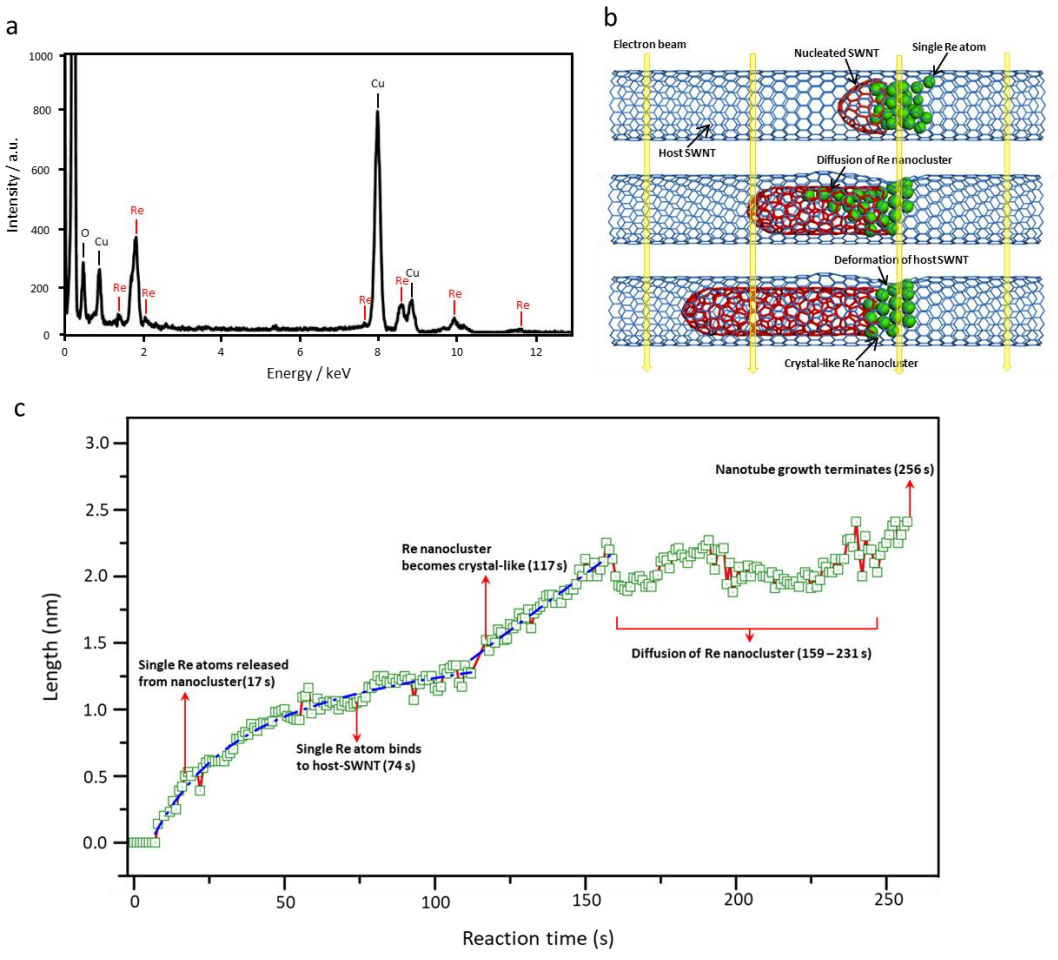

Figure 3. a). EDX spectroscopy confirms the identity of the metal clusters within the SWNT as Re; Cu-peaks are due to the TEM specimen grid. b) Schematics of the e-beam stimulated SWNT growth catalyzed by Re nanocluster. c) Plot showing the changing length of the growing nanotube measured by AC-HRTEM as a function of time. The growth starts from 7 s. The exponential decay function from 7 s to 112 s includes the Nucleation Stage (7 s-17 s) and Growth Stage 1 (17 s–112 s). The linear increase from 113 s-159 s is Growth Stage 2. Blue dashed lines are fitted by an exponential decay function and a linear equation respectively. The key events during the growth of the SWNT are highlighted by red arrows. The error in the measured length for each data point is ± 0.03 nm due to the size of the pixels in the individual TEM images; the error of the reaction times given for each data point is ± 1.0 s due to the exposure time used.

The Nucleation Stage (7 s–17 s) and Growth Stage 1 (Figure 2, 17 s-112 s) are described by an exponential function (nanotube length, l, nm; time, t, s; variance R2 = 0.967; Figure 3):

$$l = -0.96 \times e^{\left(-\frac{t}{110.53}\right)} - 0.95 \times e^{\left(-\frac{t}{19.63}\right)} + 1.63$$

where the Re nanocluster continues re-shaping and re-structuring, switching between crystal-like and liquid-like states (Figure 2, 7 s-103 s frames). The individual Re atoms increasingly engage in interactions with the host SWNT (Figure 2, green arrows). In this stage, the SWNT grows on the interface between the Re nanocluster and the SWNT indicating the diffusion of carbon atoms through the body of the Re nanocluster.[8,22] Towards the end of this period, the rate of new nanotube growth decelerates due to the depletion of readily available atoms of carbon augmented by the energy barrier for SWNT formation, which is a common characteristic of such chemical reactions.

Next, in Growth Stage 2 (Figure 3, 113 s-159 s) described by the linear function (R2 = 0.944):

$$l = 0.017 \times t - 0.52$$

the behavior of the catalyst nanocluster is strikingly different: Re atoms become ordered into a stable crystal-like lattice (Figure 2, 113 s-159 s frames), and the wall of the growing nanotube appears to emanate from a specific facet of the Re nanocrystal (Figure 2, blue arrows), resulting in a spurt of growth with a constant rate of ~0.02 nm/s, which indicates the catalytic growth of the SWNT in Growth Stage 2 is a zero-order chemical reaction. This observation is more consistent with the surface diffusion rather than the body diffusion mechanism in Stage 1.[23] This is consistent with the expectation that an ordered atomic metal lattice can provide a stable surface effectively lowering the energy barrier for SWNT formation. The degree of crystallinity of the Re cluster in the two growth stages is quantified and discussed in Figure S6 (Supporting Information). In similar fashion to Growth Stage 1, single Re atoms released from the cluster play an important role – associated with the sites of defects in the host SWNT, they act as a vehicle for drawing carbon atoms from the host SWNT to the nanocatalyst. These dynamic Re single atoms are observed only when the Re cluster is reacting with the host SWNT as shown in Figure S4 (Supporting Information). The extensive bonding between the Re atoms of the cluster with the carbon atoms of the host SWNT could reduce the binding energy between Re atoms in the cluster and thus make the Re atoms on the surface easier to dissociate from the cluster. In addition, individual Re-atoms are highly mobile and can diffuse along the newly grown nanotube, interacting with carbon atoms, then diffusing back to re-join the nanocluster (Figure 2, 159 s-231 s frames), which affects the crystallinity of the Re nanocluster and further interrupts the catalysis process demonstrating the strong correlation between the atomic structure and the catalytic activity of the nanocatalyst (Figure. 3b). Similar metal catalyst diffusion effects during the growth of CNT were observed for bigger metal nanoparticles of ~8 nm.[24] Finally, the nanotube growth is halted by a steric clash with another nanotube growing from a neighboring nanocluster, and when all Re atoms are gathered

back within the nanocluster the precise length of the final nanotube can be measured to be 2.5 nm (Figure 2, 256 s frame). The defect caused by the gradual loss of carbon atoms of the host SWNT is healed via reconstruction of host SWNT lattice, thus causing deformation where the single Re atoms interact with the host SWNT, as explained in Figure S5 (Supporting Information). The diameter of the newly formed SWNT is determined by the diameter of the Re cluster and additionally restricted by the host SWNT. Chiral index of the newly formed SWNT is determined to be (4, 8) (Figures S2, S3).

The observed slow nucleation followed by fast growth bears a striking resemblance to CVD growth inferred from ETEM and other related measurements.[4-10] However, unlike ETEM and other methods, *ChemTEM* imaging follows the entire dynamics of the nanocatalyst at the atomic level simultaneously with the growth of the nanotube, revealing strong correlation between the growth rate in real time and the atomic structure of the nanocatalyst. We demonstrate that the nucleus of the nanotube (carbon cap) and the nanocatalyst both undergo highly dynamic transformations, which substantiates the theoretical prediction that the metal nanocatalyst undergoes drastic dynamics during SWNT growth.[25] Thus, the traditional view that the carbon cap restructures extensively until it reaches an optimum binding with the catalyst surface, which remains static, appears to be an oversimplification. Our observations suggest that the nanotube nucleation process can be described more accurately as a symbiotic relationship between the carbon shell and the metal nanocluster, such that they affect each other and adapt to each other's structure at the same time, until a mutually stable configuration is reached. The observed fast linear growth correlates with the crystal-like atomic structure of the Re nanocluster and is consistent with epitaxial mechanisms proposed for CVD.[9,10] Another significant observation, which can be revealed only by *ChemTEM* is the active participation of single metal atoms in the nanotube formation process.

Dissociation of individual atoms from the parent metal nanocluster was proposed for heterogeneous nanocatalysis, and here we demonstrate directly that single metal atoms play a role in the formation of the nanotube.[26] Being chemically active, single Re atoms appear to activate carbon atoms in the host-SWNT and may be responsible for delivery of carbon to the nanocluster. Furthermore, single atoms of Re migrate over long distances and may catalyze transformation far away from the catalytic nanocluster, thus putting the classical division of the nanotube growth mechanisms into two simple categories – the base-growth and the tip-growth into question. The 'roaming' metal atoms appear to play a significant role during the nanocatalysis, which could be revealed only through the *ChemTEM* measurements (17 s, 26 s, Figure 2). The observation of these single Re atoms proves the theoretical prediction that the metal nanocluster could release the 'dynamic single atom' during the catalytic reaction which promotes the catalytic process.[27,28]

In this study, we directly image the parasitic growth of SWNT catalyzed by Re metal nanoclusters and stimulated by e-beam, in real time and with atomic resolution. In contrast to ETEM and liquid cell TEM where the impact of the e-beam is treated as an undesirable and unavoidable side effect, our approach directly harnesses the energy transfer from the e-beam to the atoms to initiate specific chemical reactions. Time-series imaging reveals that nanotube growth on Re nanoclusters promoted by the e-beam exhibit features resembling catalytic CVD processes. The symbiotic relationship between the nanocatalyst and nanotube, resembling a mechanism predicted in one the theoretical studies[29], demonstrates directly that the efficiency of nanotube formation depends on the crystalline order of the metal atoms in the nanocatalyst, which improves the mechanistic understanding of nanotube nucleation and growth. In addition, we observe directly the highly dynamic single Re atoms during the growth of the SWNT which appear to contribute

to and promote the catalytic process, as hypothesized previously for many reactions on metal nanoclusters or nanoparticles.

Materials and Methods. *Synthesis of Re@SWNT.* Arc-discharge SWNTs were annealed in air to open their termini. A three-fold excess by weight of $Re_2(CO)_{10}$ and the freshly opened SWNTs were sealed under vacuum in a quartz ampoule and heated at a temperature slightly above the vaporisation point of $Re_2(CO)_{10}$ (150 °C) for 3 days to ensure complete penetration of the SWNT by the $Re_2(CO)_{10}$ vapors. The $Re_2(CO)_{10}$ molecules were then decomposed into metal clusters inside the nanotubes either thermally (i.e., by heating above their decomposition temperature) or under the e-beam of TEM. In both cases, small clusters of metals are formed within SWNTs

Characterization. The Re@SWNT sample was dispersed in methanol and drop-cast onto lacey carbon- carbon coated copper TEM grids. Time-series AC-HRTEM images were carried out on an image-side C_s-corrected FEI Titan 80–300 TEM operated at 80 kV at room temperature. The TEM specimen was heated in air at 150 °C for 5 min shortly before insertion into the TEM column. The electron flux applied to the samples was 1×10^6 $e^-/nm^2 \cdot s$, with exposure times of either 0.5 s or 1.0 s. Local energy dispersive X-ray spectroscopy (EDX) was carried on a JEOL 2100F operated at 100 kV. The Re cluster catalyzed growth of carbon structures stimulated by the 80 keV e-beam is reproducible within our study, from sample to sample and area to area, in which we are careful to control the parameters of the e-beam and the size of the Re clusters by the SWNT confinement (variable parameters, such as the electron beam dose rate and total dose, or the size of the Re cluster may influence the overall timescale of the process, but not the principal mechanism).

ASSOCIATED CONTENT

Supporting Information.

Additional TEM images of the sample and time series; analysis of the newly formed SWNT (file type, PDF)

Supplementary video 1: the parasitic growth of SWNT catalyzed by sub-nanometre Re cluster stimulated by e-beam (file type, .AVI video)

AUTHOR INFORMATION

Corresponding Author

* (U.K.) E-mail: ute.kaiser@uni-ulm.de

* (A.N.K.) E-mail: Andrei.Khlobystov@nottingham.ac.uk

Notes

The authors declare no competing financial interest.

ACKNOWLEDGMENT

K.C. gratefully acknowledges China Scholarship Council (CSC) for financial support. J.B. and U.K. gratefully acknowledge the support of the "Graphene Flagship" and DFG SPP "Graphene" as well as the DFG and the Ministry of Science, Research and the Arts (MWK) of Baden-Wuerttemberg within the frame of the SALVE (Sub Angstrom Low Voltage Electron microscopy) project. T.W.C. and A.N.K. acknowledge ERC Consolidator and EPSRC Grants for financial support, and the Nanoscale & Microscale Research Centre (nmRC), University of Nottingham, for access to instrumentation.

REFERENCES

(1) Reina, A.; Jia, X.; Ho, J.; Nezich, D.; Son, H.; Bulovic, V.; Dresselhaus, M. S.; Kong, J. *Nano Lett.* **2008**, *9,* 30-35.

(2) Che, G.; Lakshmi, B. B.; Martin, C. R.; Fisher, E. R. Ruoff, R. S. *Chem. Mater.* **1998**, *10*, 260–267.

(3) Reinhold-López, K.; Braeuer, A.; Popovska, N. Leipertz A. *Optics express.* **2010** *18*. 18223-18228.

(4) Yoshida, H.; Takeda, S.; Uchiyama, T.; Kohno, H.; Homma, Y. *Nano Lett.* **2008**, *8,* 2082-2086.

(5) Lin, M.; Tan, J. P. Y.; Boothroyd, C.; Loh, K. P.; Tok, E. S.; Foo, Y.-L. *Nano Lett.* **2006**, *6*, 449-452.

(6) Dai, H.; Rinzler, A. G.; Nikolaev, P.; Thess, A.; Golbert, D. T.; Smalley, R. E. *Chem. Phys. Lett.* **1996**, *260,* 471-475.

(7) Reich, S.; Li, L.; Robertson, *J. Chem. Phys. Lett.* **2006**, *421,* 469-472.

(8) Rodríguez-Manzo, J. A.; Terrones M.; Terrones, H.; Kroto, H. W.; Sun, L.; Banhart, F. *Nat. Nanotech.* **2007**, *2*, 307-311.

(9) Chiang, W.-H.; Sankaran, R. M. *Nat. Mater.* **2009**, *8*, 882-886.

(10) Yang, F.; Wang, X.; Zhang, D.; Yang, J.; Luo, D.; Xu, Z.; Wei, J.; Wang, J.-Q.; Xu, Z.; Peng, F.; Li, X.; Li, R.; Li, Y.; Bai, X.; Ding, F.; Li, Y. *Nature* **2014**, *510,* 522-524.

(11) Skowron, S. T.; Chamberlain, T. W.; Biskupek, J.; Kaiser, U.; Besley, E.; Khlobystov, A. N.; *Acc. Chem. Res.* **2017**, *50*, 1797–1807.

(12) Chuvilin, A.; Khlobystov, A. N.; Obergfell, D.; Haluska, M.; Yang, S.; Roth, S.; Kaiser, U. *Angew. Chem. Int. Ed.* **2010,** *49*, 193-196.

(13) Zoberbier, T.; Chamberlain, T. W.; Biskupek, J.; Navaratnarajah, K.; Eyhusen, S.; Bichoutskaia, E.; Kaiser, U.; Khlobystov, A. N. *J. Am. Chem. Soc.* **2012**, *134*, 3073-3079.

(14) Skowron, S. T.; Lebedeva, I. V.; Popov, A. M.; Bichoutskaia, E. *Nanoscale,* **2013**, *5,* 6677-6692.

(15) Chamberlain, T. W.; Biskupek, J.; Skowron, S. T.; Markevich, A. V.; Kurasch, S.; Reimer, O.; Walker, K. E.; Rance, G. A.; Feng, X.; Müllen, K.; Turchanin, A.; Lebedeva, M. A.; Majouga, A. G.; Nenajdenko, V. G.; Kaiser, U.; Besley, E.; Khlobystov, A. N. *ACS Nano* **2017**, *11*, 2509–2520.

(16) Cao, K; Zoberbier T.; Biskupek, J.; Botos, A.; McSweeney, R. L.; Kurtoglu, A.; Stoppiello, C. T.; Markevich, A. V.; Besley, E.; Chamberlain, T. W.; Kaiser, U. Khlobystov A. N. *Nat. Comm.* **2018**, *9*, 3382

(17) Botos, A.; Biskupek, J.; Chamberlain, T. W.; Rance, G. A.; Stoppiello, C. T.; Sloan, J.; Liu, Z.; Suenaga, K.; Kaiser, U.; Khlobystov, A. N. *J. Am. Chem. Soc.* **2016**, *138*, 8175–8183.

(18) Chuvilin, A.; Kaiser, U.; Bichoutskaia, E.; Besley, N. A.; Khlobystov, A .N. *Nat. Chem.* **2010**, *2,* 450-453.

(19) Chuvilin, A.; Bichoutskaia, E.; Gimenez-Lopez, M. C.; Chamberlain, T.W.; Rance, G.A.; Kuganathan, N.; Biskupek, J.; Kaiser, U.; Khlobystov, A. N. *Nat. Mater.* **2011**, *10*, 687-692.

(20) Skowron, S. T.; Koroteev, V. O.; Baldoni, M.; Lopatin, S.; Zurutuza, A.; Chuvilin, A.; Besley, E. *Carbon* **2016**, *105*, 176-182.

(21) Chamberlain, T. W.; Meyer, J. C.; Biskupek, J.; Leschner, J.; Santana, A.; Besley, N.A.; Bichoutskaia, E.; Kaiser, U.; Khlobystov, A. N.; *Nat. Chem.* **2011**, *3*, 732-737.

(22) Pohl, D.; Schäffel, F.; Rümmeli, M. H.; Mohn, E.; Täschner, C.; Schultz,; L. Kisielowski, C.; Rellinghaus, B. *Phys. Rev. Lett.* **2011,** *107*, 185501.

(23) Abild-Pedersen, F.; Nørskov, J. K.; Rostrup-Nielsen, J. R.; Sehested, J.; Helveg, S.; *Phys. Rev. B* **2006**, *73*, 115419.

(24) Moseler, M.; Cervantes-Sodi, F.; Hofmann, S.; Csányi, G.; Ferrari A. C. *ACS Nano* **2010**, *4*, 7587–7595.

(25) Ohta, Y.; Okamoto, Y.; Irle, S.; Morokuma, K. *ACS nano* **2008**, *2*, 1437–1444.

(26) Patera, L. L.; Bianchini, F.; Africh, C.; Dri, C.; Soldano, G.; Mariscal, M. M.; Peressi, M.; Comelli, G. *Science* **2018**, *359*, 1243-1246.

(27) Liu, J-C.; Wang, Y-G.; Li, J. *J. Am. Chem. Soc.* **2017**, *139*, 6190-6199.

(28) Wang, Y-G.; Mei, Do.; Glezakou, V-A., Li, J.; Rousseau, R. *Nat. Comm.* **2015**, *6*, 6511.

(29) Shibuta, Y.; Maruyama, S.; *Chem. Phys. Lett.* **2003**, *382*, 381.

Table of Contents Graphic